

Ultralow drive voltage silicon traveling-wave modulator

Tom Baehr-Jones,^{1,*} Ran Ding,¹ Yang Liu,¹ Ali Ayazi,¹ Thierry Pinguet,¹ Nicholas C. Harris,¹ Matt Streshinsky,¹ Poshen Lee,¹ Yi Zhang,¹ Andy Eu-Jin Lim,² Tsung-Yang Liow,² Selin Hwee-Gee Teo,² Guo-Qiang Lo,² and Michael Hochberg³

¹Department of Electrical Engineering, University of Washington, Campus Box 352500, Seattle, Washington 98195, USA

²Institute of Microelectronics, Agency for Science, Technology and Research (A*STAR), Singapore 117685, Singapore

³Department of Electrical and Computer Engineering, University of Delaware, 140 Evans Hall, Newark, DE 19716, USA

*baehrjt@u.washington.edu

Abstract: There has been great interest in the silicon platform as a material system for integrated photonics. A key challenge is the development of a low-power, low drive voltage, broadband modulator. Drive voltages at or below 1 Vpp are desirable for compatibility with CMOS processes. Here we demonstrate a CMOS-compatible broadband traveling-wave modulator based on a reverse-biased pn junction. We demonstrate operation with a drive voltage of 0.63 Vpp at 20 Gb/s, a significant improvement in the state of the art, with an RF energy consumption of only 200 fJ/bit.

©2012 Optical Society of America

OCIS codes: (250.3140) Integrated optoelectronic circuits; (250.7360) Waveguide modulators.

References and links

1. M. Lipson, "Guiding, modulating, and emitting light on silicon - challenges and opportunities," *J. Lightwave Technol.* **23**(12), 4222–4238 (2005).
2. A. Liu, R. Jones, L. Liao, D. Samara-Rubio, D. Rubin, O. Cohen, R. Nicolaescu, and M. Paniccia, "A high-speed silicon optical modulator based on a metal-oxide-semiconductor capacitor," *Nature* **427**(6975), 615–618 (2004).
3. L. Liao, A. Liu, D. Rubin, J. Basak, Y. Chetrit, H. Nguyen, R. Cohen, N. Izhaky, and M. Paniccia, "40 Gbit/s silicon optical modulator for high-speed applications," *Electron. Lett.* **43**(22), 1196–1197 (2007).
4. D. J. Thomson, F. Y. Gardes, Y. Hu, G. Mashanovich, M. Fournier, P. Grosse, J.-M. Fedeli, and G. T. Reed, "High contrast 40Gbit/s optical modulation in silicon," *Opt. Express* **19**(12), 11507–11516 (2011).
5. D. J. Thomson, F. Y. Gardes, J.-M. Fedeli, S. Zlatanovic, Y. Hu, B. P. P. Kuo, E. Myslivets, N. Alic, S. Radic, G. Z. Mashanovich, and G. T. Reed, "50-Gb/s silicon optical modulator," *IEEE Photon. Technol. Lett.* **24**(4), 234–236 (2012).
6. M. R. Watts, W. A. Zortman, D. C. Trotter, R. W. Young, and A. L. Lentine, "Low-voltage, compact, depletion-mode, silicon Mach-Zehnder modulator," *IEEE J. Sel. Top. Quantum Electron.* **16**(1), 159–164 (2010).
7. W. M. J. Green, M. J. Rooks, L. Sekaric, and Y. A. Vlasov, "Ultra-compact, low RF power, 10 Gb/s silicon Mach-Zehnder modulator," *Opt. Express* **15**(25), 17106–17113 (2007).
8. Q. F. Xu, B. Schmidt, S. Pradhan, and M. Lipson, "Micrometre-scale silicon electro-optic modulator," *Nature* **435**(7040), 325–327 (2005).
9. G. Li, X. Zheng, J. Yao, H. Thacker, I. Shubin, Y. Luo, K. Raj, J. E. Cunningham, and A. V. Krishnamoorthy, "25Gb/s 1V-driving CMOS ring modulator with integrated thermal tuning," *Opt. Express* **19**(21), 20435–20443 (2011).
10. T. Baehr-Jones, M. Hochberg, C. Walker, Eric Chan, D. Koshinz, W. Krug, and A. Scherer, "Analysis of the tuning sensitivity of silicon-on-insulator optical ring resonators," *J. Lightwave Technol.* **23**(12), 4215–4221 (2005).
11. X. Z. Zheng, D. Patil, J. Lexau, F. Liu, G. L. Li, H. Thacker, Y. Luo, I. Shubin, J. D. Li, J. Yao, P. Dong, D. Z. Feng, M. Asghari, T. Pinguet, A. Mekis, P. Amberg, M. Dayringer, J. Gainsley, H. F. Moghadam, E. Alon, K. Raj, R. Ho, J. E. Cunningham, and A. V. Krishnamoorthy, "Ultra-efficient 10 Gb/s hybrid integrated silicon photonic transmitter and receiver," *Opt. Express* **19**(6), 5172–5186 (2011).
12. <http://www.luxtera.com/>.
13. T. Pinguet, B. Analui, E. Balmaier, D. Guckenberger, M. Harrison, R. Koumans, D. Kucharski, Y. Liang, G. Masini, A. Mekis, S. Mirsaidi, A. Narasimha, M. Peterson, D. Rines, V. Sadagopan, S. Sahni, T. J. Sleboda, D. Song, Y. Wang, B. Welch, J. Witzens, J. Yao, S. Abdalla, S. Gloeckner, P. De Dobbelaere, and G. Capellini, "Monolithically integrated high-speed CMOS photonic transceivers," *Proc. 5th IEEE Int. Conf. Group IV Photonics* 362–364 (2008).

14. B. Razavi, *Design of Analog CMOS Integrated Circuits* (McGraw-Hill, 2001).
15. G. Kim, J. W. Park, I. G. Kim, S. Kim, S. Kim, J. M. Lee, G. S. Park, J. Joo, K.-S. Jang, J. H. Oh, S. A. Kim, J. H. Kim, J. Y. Lee, J. M. Park, D.-W. Kim, D.-K. Jeong, M.-S. Hwang, J.-K. Kim, K.-S. Park, H.-K. Chi, H.-C. Kim, D.-W. Kim, and M. H. Cho, "Low-voltage high-performance silicon photonic devices and photonic integrated circuits operating up to 30 Gb/s," *Opt. Express* **19**(27), 26936–26947 (2011).
16. J. Ding, H. Chen, L. Yang, L. Zhang, R. Ji, Y. Tian, W. Zhu, Y. Lu, P. Zhou, and R. Min, "Low-voltage, high-extinction-ratio, Mach-Zehnder silicon optical modulator for CMOS-compatible integration," *Opt. Express* **20**(3), 3209–3218 (2012).
17. J. Macario, Peng Yao, R. Shireen, C. A. Schuetz, Shouyuan Shi, and D. W. Prather, "Development of electro-optic phase modulator for 94 GHz imaging system," *J. Lightwave Technol.* **27**(24), 5698–5703 (2009).
18. Y. Tang, H.-W. Chen, S. Jain, J. D. Peters, U. Westergren, and J. E. Bowers, "50 Gb/s hybrid silicon traveling-wave electroabsorption modulator," *Opt. Express* **19**(7), 5811–5816 (2011).
19. P. Dong, L. Chen, and Y.-K. Chen, "High-speed low-voltage single-drive push-pull silicon Mach-Zehnder modulators," *Opt. Express* **20**(6), 6163–6169 (2012).
20. <http://www.ime.a-star.edu.sg/PPSSite/index.asp>.
21. T.-Y. Liow, K.-W. Ang, Q. Fang, J.-F. Song, Y.-Z. Xiong, M.-B. Yu, G.-Q. Lo, and D.-L. Kwong, "Silicon modulators and germanium photodetectors on SOI: monolithic integration, compatibility, and performance optimization," *IEEE J. Sel. Top. Quantum Electron.* **16**(1), 307–315 (2010).
22. J. Witzens, T. Baehr-Jones, and M. Hochberg, "Design of transmission line driven slot waveguide Mach-Zehnder interferometers and application to analog optical links," *Opt. Express* **18**(16), 16902–16928 (2010).
23. G. Roelkens, D. Van Thourhout, and R. Baets, "High efficiency Silicon-on-Insulator grating coupler based on a poly-Silicon overlay," *Opt. Express* **14**(24), 11622–11630 (2006).
24. R. Soref and B. R. Bennett, "Electrooptical effects in silicon," *IEEE J. Quantum Electron.* **23**(1), 123–129 (1987).

1. Introduction

Achieving efficient modulation in the silicon material system has always been one of the key challenges of silicon photonics [1]. Since the first multi-Gb/s silicon modulator was demonstrated by Liu et al in 2004 [2], several approaches have been pursued. Reverse-bias pn Mach-Zehnder modulators exhibit the highest bandwidths, with 3 dB bandwidths of 30 GHz demonstrated, and 50 Gb/s speeds achieved [3–5], but relatively poor modulation figures of merit, with the lowest $V\pi L$ shown 1.1 V-cm [6]. PIN injection modulators achieve lower $V\pi L$ figures of merit, such as 0.035 V-cm, which enables dramatically shorter devices, but have bandwidth limitations; 10 Gb/s operation is possible, but only through techniques such as pre-emphasis. Energy consumption in the PIN modulator also remains high. The lowest energy per bit reported is 5 pJ/bit [7].

One approach taken to lowering the required drive voltage and power consumption has been to use ring resonator geometries [8]. Recently, Li et al demonstrated a 25 Gb/s ring modulator with energy consumption only 7 fJ/bit [9]. One issue with optical resonators, however, is their temperature sensitivity [10]; a shift in 20° C can give a resonance change of around 1 nm. In a realistic system, with a silicon photonics component in close proximity to a CPU or memory chip, such temperature shifts are anticipated. The aforementioned ring modulator would require 5 mW of tuning power in order to counteract this level of drift, which would amount to an extra 200 fJ/bit at 25 Gb/s. In situations where the temperature of the silicon can change substantially, the realizable energy per bit consumption for resonator-based modulators will be much higher than the theoretical limits, due to the cost of thermal tuning. Typical modulator driver circuitry for ring modulators will consume additional power; recently 135 fJ/bit power consumption was reported [11]. In eventual systems, it is thus likely that net power consumption for ring modulator based transmitters will be at least 100-300 fJ/bit.

Though they have higher power consumption and drive voltage as compared to ring modulators, Mach-Zehnders remain interesting for several reasons. Most importantly, a balanced Mach-Zehnder is relatively temperature insensitive, and so no additional power would needed to be expended to compensate for temperature drift. Another advantage is the lack of sensitivity of the Mach-Zehnder to the particular optical input wavelength. Ring modulators require a locking between the resonance peak and the laser wavelength of perhaps 10 pm or better [9], but a Mach-Zehnder can easily operate across 10 nm of spectrum or more. It is worth noting that one of the first silicon photonics products, a 40 Gb/s data-link, utilized Mach-Zehnders, not ring modulators [12,13].

It is desirable to achieve modulation in a Mach-Zehnder with V_{pp} values below 1 V, as this is then directly compatible with the typical transistor voltages found in modern CMOS processes [14]. There has been recent progress in lowering the drive voltage in traveling-wave Mach-Zehnder modulators, with on-chip voltages of 2.4 V_{pp} achieved at speeds up to 30 Gb/s [15]. A lower drive voltage of 1 V_{pp} was also achieved at 12.5 Gb/s [16]. Here we show that the drive voltage can be lowered at higher speeds as well. We extend the length of a traveling-wave device [17–19] to 5 mm while maintaining high bandwidth through careful RF design. We demonstrate operation at 0.63 V_{pp} at 20 Gb/s, which implies an energy consumption of 200 fJ/bit. A drive voltage of 1 V_{pp} can also be utilized in order to minimize device insertion losses.

2. Device geometry and fabrication

Fabrication occurred at the Institute of Microelectronics (IME)/A*STAR [20,21]. The starting material was an 8" Silicon-on-Insulator (SOI) wafer from SOITEC, with a Boron-doped top silicon layer of around 10 ohm-cm resistivity and 220 nm thickness, a 2 μ m bottom oxide thickness, and a 750 ohm-cm handle silicon wafer, needed for RF performance [22]. Rib waveguides used for modulation were formed using an anisotropic dry etch. In all cases 248 nm photolithography was utilized. A lateral pn junction was defined in the center of the rib with p and n implants on the exposed silicon, prior to any oxide fill. Additional p++ and n++ implants were utilized for ohmic contact formation, followed by a rapid thermal anneal at 1030 °C for 5 s for Si dopant activation, and then by the formation of contact vias and two levels of aluminum. Chemical-mechanical planarization (CMP) was not utilized. The schematic cross-section of the final device is shown in Fig. 1. Additional etch steps, not shown here, were used to define grating couplers [23], used to couple to a fiber mode, and channel waveguides, used for routing. Over 40 dies were simultaneously fabricated. The data presented here is from a die at the center of the wafer.

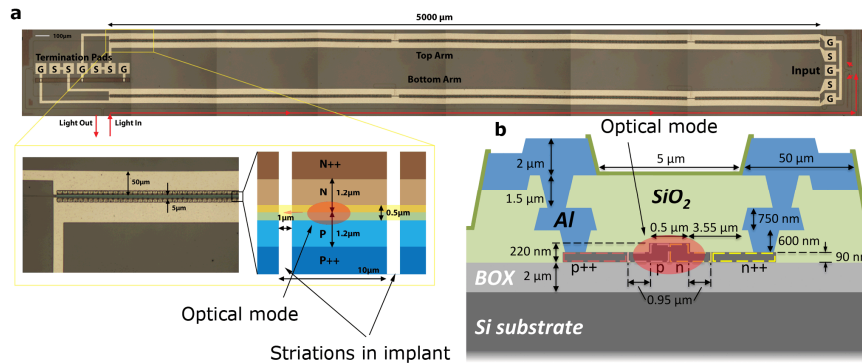


Fig. 1. Device structure and fabrication. (a) Optical micrograph of the traveling-wave device, with the inset showing the detailed junction geometry. Note that termination is achieved with a GSSGSSG configuration, providing a 25 Ω termination on each arm. The inset at highest magnification is a rendering of the layout file used in fabrication. (b) A cross-section of the fabricated device is shown, with the two metal layers indicated, as well as the rib waveguide structure and the lateral pn junction. The current for the RF mode propagates largely in the thicker top metal layer due to striations in the pn junction and lower metal layer, lowering ohmic losses.

A coplanar metal strip geometry was utilized, along with the lateral pn junction, to construct a traveling-wave Mach-Zehnder modulator. Striations were used in the pn junction region to ensure that current flowed in the metal strips, as opposed to the junction itself, as detailed in Fig. 1(a). The two arms have two independent transmission lines, which enable differential drive of the device. The device operated in reverse-bias, with the voltage-dependent shift in depletion region causing an induced effective index shift in the waveguide. We chose implant doses to provide a peak dopant concentration of $5 \times 10^{17} \text{ cm}^{-3}$ for the n

region, and $7 \times 10^{17} \text{ cm}^{-3}$ for the p region. Higher concentrations can achieve lower $V\pi L$ values, but at the expense of increased excess loss [24].

3. Device characterization

The 5 mm traveling-wave Mach-Zehnder was first characterized at DC, by measuring the transmission spectrum as a function of wavelength for varying reverse-bias voltages. The phase shift in each arm as a function of voltage could be computed from the observed shift in fringes, shown in Fig. 2. The degradation of $V\pi L$ at higher voltages is as expected due to the nonlinearity of the junction. The insertion loss for the Mach-Zehnder is $8.7 \pm 0.7 \text{ dB}$, corresponding to an approximate excess loss from the implants of 10 dB/cm . This is higher than the value we predicted of 6.7 dB/cm . Losses from the y-junctions were approximately 2.6 dB , with the rest of the loss due to the waveguide itself. Current flows around $1 \mu\text{A}$ or lower were seen for reverse biases up to 5 V . For forward bias, current flows remained below $10 \mu\text{A}$ for forward biases up to 0.5 V . This is as expected, due to the built-in voltage of the junction, and suggests that high-bandwidth operation can still be expected for small forward-biases. Note that for both the top and bottom arms seen in Fig. 1, the n-type material is directly connected to the S lines; therefore, positive voltage would result in a reverse-bias. The Mach-Zehnder was intentionally unbalanced by a waveguide length of $100 \mu\text{m}$, to enable biasing of the modulator by tuning the input wavelength. This accounts for the fringes seen in the spectrum in Fig. 2. Finally, C-V measurements were taken, with the capacitance due to the metal strips normalized out with control structures, as shown in Fig. 2. The capacitance due to the pn junction was found to be relatively frequency insensitive up to around 200 MHz , which was the limit of our measurement technique.

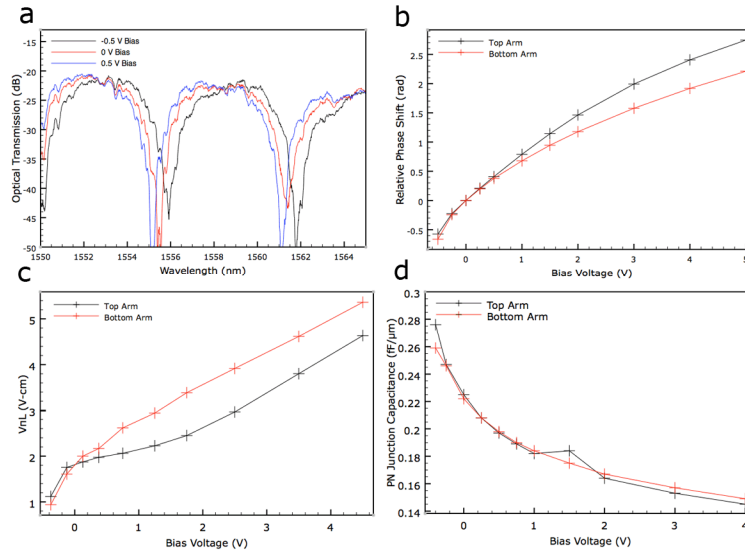


Fig. 2. Device dc characterization. (a) Typical device transmission spectrum is shown for varying applied voltages. Only one arm has a bias applied in these curves. (b) Phase shift as a function of voltage for the top and bottom arm of a typical device is shown, determined by tracking the shift in fringe locations as bias voltage was altered. Note the y axis is in radians, not multiples of π radians. (c) The small-signal $V\pi L$ value, which can be directly calculated from the relative phase shift, is shown as a function of voltage for both arms. (d) C-V curves on both arms of a device. These measurements are normalized against metal-only control structures, and should thus reflect only the pn junction capacitance in addition to a slight contribution from fringing fields in the rib waveguide.

The RF properties of the traveling-wave device are determined by a combination of the inductive path, which is through the metal traces, and the net capacitance of the metal traces

as well as the pn junction. To fully understand the RF characteristics of the device, a metal control structure consisting of just the coplanar metal strips was characterized. We report the following values at 10 GHz, as it is the most relevant frequency, being at the bandwidth limitation. An impedance of $61-5i \Omega$ at 10 GHz was determined based on the observed S21 and S11 values, with RF losses of 3.8 dB/cm. This suggests an inductance of 457 nH/m at 10 GHz, with series resistances of 4.9 k Ω /m and capacitances of 0.12 nF/m. Another significant quantity for RF performance is the sheet resistance of the partially etched silicon. This was measured to be 10 kohm/ \square for the partially etched p-type silicon, and 7 kohm/ \square for the partially etched n-type silicon. The clearance between the edge of the rib waveguide, as seen in Fig. 1, and the p + + and n + + regions was 0.95 μ m. This corresponds to a resistance of 1.6 Ω -cm, which becomes a sharp limitation at higher RF frequencies. Future devices could enjoy higher RF bandwidths by using an intermediate doping step to lower this resistance.

By combining the inductance and series resistance from the metal control structure, with the capacitance from the control structure and the junction capacitance, one can calculate the RF parameters of the full traveling-wave modulator. The net line impedance at 10 GHz was 37-1i Ω [22], with RF losses of 10.8 dB/cm. There will be minimal changes in impedance within the 1-10 GHz range. The RF effective index is also 3.75, close to the optical group index 3.86 for the rib waveguide. These values were consistent with the estimated RF parameters from observing the S11 and S21 values of the complete traveling-wave device. The primary bandwidth limitation for electrooptic modulation is the RF loss. It can readily be shown that the 3 dB point in an electrooptic S21 will be reached when there is around 6 dB of RF loss at the end of the transmission line, which is consistent with the value we observed. Velocity mismatch is not a major limitation. Both 50 Ω and 25 Ω lines can drive or terminate a 37-1i Ω line with tolerable return losses. An integrated modulator driver should also be able to drive the line directly.

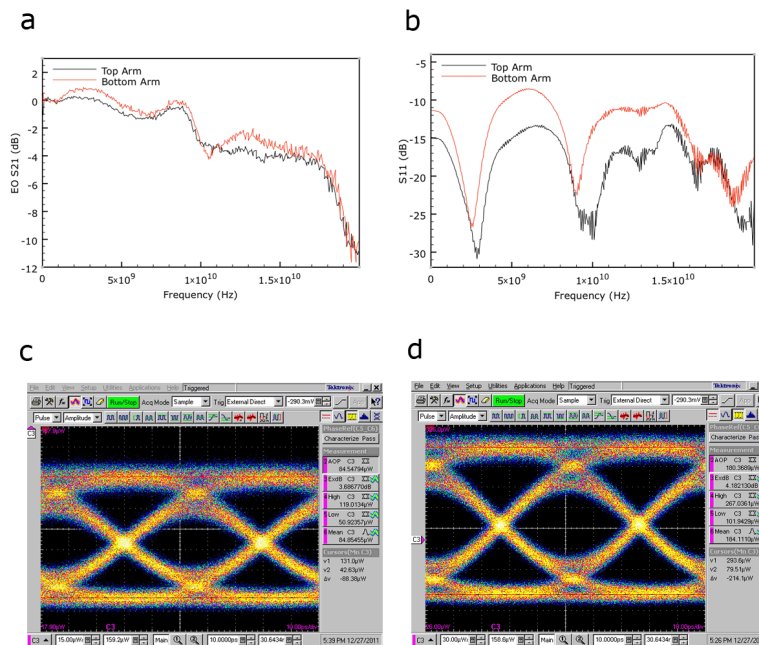


Fig. 3. Device RF characterization. (a) Electrooptic (EO) S21 parameters of both arms of the traveling-wave 5 mm device. 3 dB bandwidths are seen at 10 GHz. (b) Device S11 seen on both arms. The value is approximately consistent with the impedance of 37-1i Ω calculated from the control structures at 10 GHz. (c) An eye pattern at 20 Gb/s is shown. A 0.63 Vpp differential drive is used, centered at 0 V, with 5 dB excess loss for a “1” bit and a 3.7 dB extinction ratio achieved. (d) An eye pattern at 20 Gb/s with 1 Vpp differential drive; an excess loss of 1.6 dB is achieved with 4.2 dB of extinction.

RF performance of the traveling-wave device was characterized by an electrooptic S21 parameter, shown in Fig. 3. A 3 dB bandwidth of 10 GHz is seen for both arms. A small amount of ripple in the spectrum is seen. This is likely due to the impedance mismatch from the line to the terminator, as well as possible cross-talk between the arms; a GS line will have a larger fringing RF field than a GSG line, and so the latter will likely be preferred in future generations of devices. A pseudo-random bit sequence (PSRBS31) was driven through the device to determine digital modulation performance. Using an input voltage of 0.63 V_{pp} at 50 Ω for differential drive on both arms, 3.7 dB of extinction was obtained. Note that the modulator is biased past quadrature in this case, causing a “1” bit to have excess loss of 5 dB. It is also possible to bias the modulator for lower loss; with a 1 V_{pp} signal, 4.2 dB extinction was achieved with 1.6 dB excess loss (Fig. 3(c)). In all cases, no DC bias was utilized; that is, the signals were centered at 0 V. However, minimal changes in the eye pattern were seen when a DC offset was added to keep the drive voltages strictly positive. This is due to the relative linearity of the pn junction response, as seen in Fig. 2, for bias voltages near 0 V. The wavelength used for the eye patterns was approximately 1555 nm, with a small level of tuning used to bias the modulator at the desired operating regime.

The RF power utilized under our experimental conditions to drive the 5 mm device can be readily computed. At an impedance of 50 Ω , an ideal 0.63 V_{pp} NRZ signal centered on 0 V carries 2 mW of power. Two such arms in parallel are required to drive the device, which in turn implies energy consumption of 20 Gb/s of 200 fJ/bit. We note that the loss due to modulator biasing, eye-pattern extinction ratio, and drive voltage can be traded off, one against the other. For example, if more extinction were desired for the 1 V_{pp} driven device, the modulator could be biased with the “1” bit near quadrature, resulting in an increased extinction ratio, though excess optical loss.

We briefly comment on the temperature sensitivity of our device. For an ideal, balanced, Mach-Zehnder modulator, there should be no temperature sensitivity at all, because the index shift induced in each arm is exactly symmetric, and so there is no relative phase change. As previously mentioned, an unbalanced device was employed here in order to facilitate testing. For a device with 100 μm of imbalance, it can readily be shown that the induced relative phase shift will be 0.06 rad/ $^{\circ}\text{C}$ [10]. On the other hand, around 1 radian of net relative phase shift occurs in the course of driving an eye pattern, as can be seen from Fig. 2. We can expect significant device performance changes when the induced relative phase shift is on the order of 25% of this value. Thus the device operating window should be around 8.3 $^{\circ}\text{C}$. By contrast, if a ring modulator requires the driving laser wavelength to remain within a 10 pm window, only a 0.2 $^{\circ}\text{C}$ operating window will be available, for the previously described ring modulator with 0.05 nm/ $^{\circ}\text{C}$ of resonance shift. Even in this unoptimized version, the Mach-Zehnder modulator should exhibit superior performance by over an order of magnitude in this key metric.

4. Conclusions

We have demonstrated 20 Gb/s modulation with drive voltages as low as 0.63 V_{pp}, corresponding to a low RF power consumption of 200 fJ/bit. Our results suggest that it is possible to build silicon-based modulators that are directly compatible with CMOS transistor voltages in even the most modern processes. One remaining challenge is lowering the insertion loss; the net loss seen for a “1” bit shown here for the 0.63 V_{pp} modulation, 13.7 dB on-chip loss, is still superior to other values shown in the literature for high-speed modulation [4]. However, it may be too high for some applications. Lowering the excess loss due to the implants, which is larger in our device than the theoretically predicted value, will be key in lowering the level of optical loss, as will optimizing passive devices such as the y-junctions.

Traditionally, Mach-Zehnders have been considered attractive for modulation, as compared to ring modulators, due to their temperature insensitivity and broad wavelength operating range. However, the large power consumption has usually made them less viable for low energy-per-bit applications. The 200 fJ/bit power consumption that we show here, however, should prompt a reexamination of this assumption. As we relate earlier in our paper,

when the supporting circuitry for ring modulators required for both tuning and driving the modulator is considered, it is inevitable that energy consumptions on the order of 200 fJ/bit or higher will be required. As a result, a traveling-wave modulator such as the one demonstrated here might prove attractive for future communications applications.

Acknowledgments

Assistance with 20 Gb/s testing from Klaus Engenhardt at Tektronix is gratefully acknowledged. The authors would like to thank Matthew Goodman of DARPA for support under the ZOE program and Gernot Pomrenke, of the Air Force Office of Scientific Research, for support under the OPSIS and PECASE programs. Lastly, the authors would like to thank Mario Panniccia and Justin Rattner, of Intel, for their support of the Institute for Photonic Integration.